CARBON NANOTUBES

DNA-guided lattice remodeling of carbon nanotubes

Zhiwei Lin[1]*†, Leticia C. Beltrán[2], Zeus A. De los Santos[1], Yinong Li[3], Tehseen Adel[4], Jeffrey A Fagan[1], Angela R. Hight Walker[4], Edward H. Egelman[2], Ming Zheng[1]*

Covalent modification of carbon nanotubes is a promising strategy for engineering their electronic structures. However, keeping modification sites in registration with a nanotube lattice is challenging. We report a solution using DNA-directed, guanine (G)-specific cross-linking chemistry. Through DNA screening we identify a sequence, $C_3GC_7GC_3$, whose reaction with an (8,3) enantiomer yields minimum disorder-induced Raman mode intensities and photoluminescence Stokes shift, suggesting ordered defect array formation. Single-particle cryo–electron microscopy shows that the $C_3GC_7GC_3$ functionalized (8,3) has an ordered helical structure with a 6.5 angstroms periodicity. Reaction mechanism analysis suggests that the helical periodicity arises from an array of G-modified carbon-carbon bonds separated by a fixed distance along an armchair helical line. Our findings may be used to remodel nanotube lattices for novel electronic properties.

Synthesis of carbon-based quantum materials can, in principle, employ rich organic chemistry to realize novel properties through atomic-precision structural engineering. More than 50 years ago, W. A. Little proposed a room-temperature organic superconductor model composed of a one-dimensional conducting chain with an array of polarizable side chains attached (*1*). Since then, numerous efforts to verify Little's proposal had been made but all have failed (*2*). In 2016 the mechanism underlying Little's model—electron attraction mediated by polarizable groups—was confirmed for the first time (*3*). The study used a single-wall carbon nanotube (SWCNT) as the one-dimensional conducting chain, along which a nanotube circuitry was constructed to provide a single polarizable "side chain." This work suggests a route to the Little model by chemically implanting polarizable groups in registration with a SWCNT lattice (*4*). However, there exists a major challenge in controlling reaction sites along the nanotube, which seems insurmountable as half the population of carbon atoms on a given SWCNT are chemically equivalent and are enantiomers of the remaining half. We report a DNA-guided chemical reaction to overcome this challenge. We screen reaction products by resonance Raman and photoluminescence (PL) spectroscopy and inspect the structures of promising candidates by single-particle cryo–electron microscopy (cryo-EM). Our findings demonstrate the feasibility of not only creating a wide range of SWCNT derivatives in general but also building a Little model in particular.

Broadly speaking, covalent modification of SWCNTs is a promising route toward organic quantum materials (*5*–*7*). With all atoms on their surfaces, SWCNTs are more amenable than other solid state materials to precision molecular engineering by wet chemistry. In addition, various chiral forms of SWCNTs made available by sorting (*8*) offer a diverse range of electronic structures for further chemical tailoring. Recently, Weisman *et al.* reported a photochemical reaction of DNA-wrapped SWCNTs with singlet oxygen that covalently links guanine (G) to the side wall of SWCNTs (*6*). Even though the chemical nature of the covalent link was not fully revealed and the structure of the reaction product was rather disordered (*9*), we are nevertheless motivated to pursue ordered SWCNT lattice modification with the goal of finding more effective ways to explore nanotube chirality and DNA sequence space.

To speed up sequence screening and to promote ordered structure formation, we have explored conditions for the guanine functionalization reaction of SWCNTs. We find that the previously reported aqueous phase photochemical reaction of Rose Bengal (RB)–mediated guanine cross-linking with SWCNTs (*6*) also works in mixed solvents containing both methanol and water. In 50% v/v methanol, the reaction proceeds slower (60 min) than that in water (15 min); further, consumption of RB sensitizer is decreased considerably and RB binding to SWCNTs—which may adversely affect DNA wrapping structures and cross-linking sites—is also minimized. All these changes should favor homogeneous product formation. Combining this new reaction condition with a previously established process (*10*) for DNA-surfactant exchange, we have devised a one-pot chemistry (Fig. 1A and figs. S1 to S5) that can efficiently react any G-containing sequence with any single-chirality SWCNT species [e.g., (6,5), (9,1), (8,3), and so on] purified independently through various techniques (*8*). Excess DNA is present during the reaction to refill exposed nanotube surfaces arising from reaction-induced DNA structure contraction, eliminating a potential source of inhomogeneous functionalization.

We have employed spectroscopic tools to monitor the reaction (Fig. 1 and figs. S6 and S7). Figures 1B to 1D present a data set from a reaction on an (8,3) enantiomer (normalized circular dichroism signal at the E_{22} = – 42 mdeg, which according to theoretical analysis corresponds to a right-handed enantiomer) (*11*). Hereafter we denote the enantiomer simply as (8,3) unless indicated otherwise. Figures 1B and 1C respectively show the expected red shift of the E_{11} absorption and PL peak after functionalization. Figure 1D shows resonance Raman spectra of unfunctionalized (black trace) and functionalized (8,3) (red trace). In addition to the well-documented D peak, we find another disorder-induced peak: the intermediate frequency mode (IFM) (*12*, *13*) at 387 cm^{-1}, with overtone 2 IFM at 775 cm^{-1} and combination modes with D: D ± IFM at 905 and 1680 cm^{-1}, respectively. There is considerable intensity enhancement of the D and IFM modes in the functionalized tubes. By contrast, 2IFM and D ± IFM peaks remain weak and unchanged after functionalization, consistent with their origin from two-phonon, second-order scattering processes (*12*).

To gain insight into the reaction mechanism, we have functionalized (8,3) using a set of DNA sequences with varying G content. With increasing G content the functionalized (8,3) shows a gradual increase in both D and IFM peak intensity (Fig. 2, A and B) in addition to more red-shifted and broadened PL and absorbance peaks (Fig. 2, C and D). These observations are consistent with a previous study which used mixed chirality tubes (*6*). However, using chirality-pure SWCNTs allows us to unambiguously determine the absorption and PL peak positions of the functionalized tube as well as calculate its absorption peak shift and Stokes shift (SS), i.e., the energy difference between the absorption and PL peak, as a function of G content or defect density. The absorption peak shift increases with G content (Fig. 2E), but its amplitude is <27 meV, about ten times as small as that typically observed for an sp^3 defect (*14*). This difference is notable considering that the defect density (≈10°/nm) in guanine-modified tubes (*15*) is about two orders of magnitude higher than that in sp^3-modified tubes (*5*). The SS also increases with defect density (Fig. 2E), a trend opposite that observed for sp^3 defects (*14*). In addition, we find a quantitative relationship between SS and full width at half maximum

[1]Materials Science and Engineering Division, National Institute of Standards and Technology, Gaithersburg, MD 20899, USA. [2]Department of Biochemistry and Molecular Genetics, University of Virginia, Charlottesville, VA 22908, USA. [3]South China Advanced Institute for Soft Matter Science and Technology, School of Emergent Soft Matter, South China University of Technology, Guangzhou 510640, China. [4]Quantum Metrology Division, National Institute of Standards and Technology, Gaithersburg, MD 20899, USA.
***Corresponding author. Email: zhiweilin@scut.edu.cn (Z.L.); ming.zheng@nist.gov (M.Z.)**
†Present address: South China Advanced Institute for Soft Matter Science and Technology, School of Emergent Soft Matter, South China University of Technology, Guangzhou 510640, China.

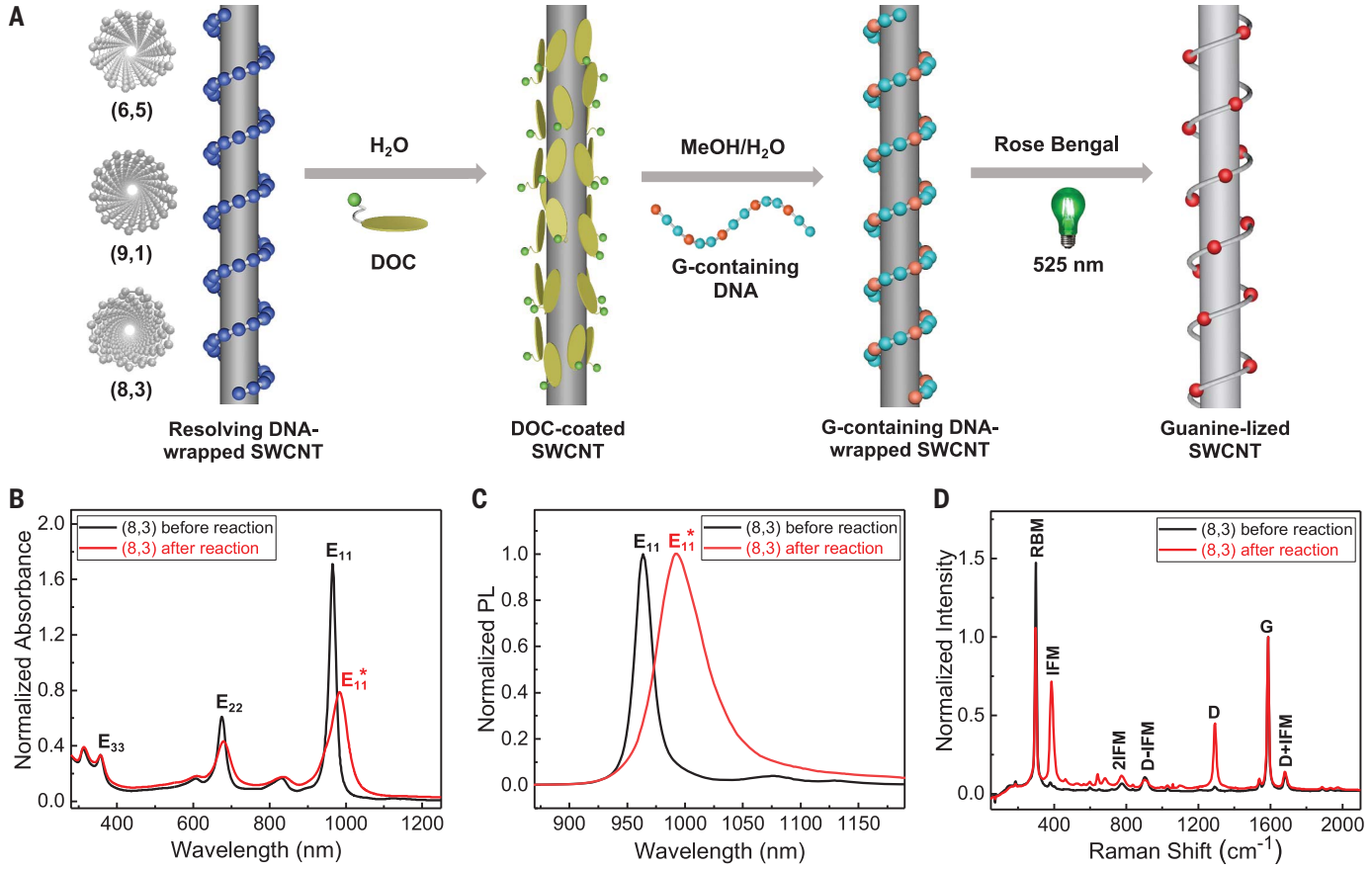

Fig. 1. One-pot photochemical reaction scheme and spectral characterization. (**A**) Reaction scheme starting from resolving DNA-wrapped to guanine-functionalized (guanine-lized) SWCNT carried out in a single pot. DOC, sodium deoxycholate. (**B**) Absorption (normalized at E_{33}). (**C**) PL (with peak intensity normalized to 1). (**D**) Resonance Raman spectra (normalized at the "G" peak) of (8,3) before and after the reaction. Spectra in (C) and (**D**) are measured with 671 nm excitation corresponding to E_{22} of (8,3). The DNA sequence used in this experiment is $(GCC)_{12}$. See fig. S8 for data shown in (B) and (C) before normalization.

(W) of the PL peaks, suggesting that modified and unmodified carbon atoms are isovalent as discussed below. In Fig. 2F we plot SS versus W^2 and fit the data well (R^2 = 0.98) with T = 349.3 K using Eq. 1, where k is the Boltzmann constant and T is the effective exciton temperature equal to or above the ambient temperature.

$$SS = \frac{W^2}{8 \ln 2\, kT} \cong 0.18 \frac{W^2}{kT} \qquad (1)$$

Eq. 1 has been used to describe excitons in two-dimensional (2D) quantum wells and 3D alloy semiconductors in which disordered isovalent substitution creates shallow traps (*16*, *17*). It attributes the observed SS to the thermalization of excitons in an inhomogeneously broadened band. Combining all of these spectroscopic observations, we exclude sp^3 defect formation by guanine functionalization and conclude that the chemistry employed creates a modified sp^2 defect that is isovalent to the original sp^2 carbon in the pristine SWCNT.

To differentiate the two types of disorders originating from the defect density itself and defect distribution pattern, we have designed a set of 15-mer G/C sequences containing two Gs separated by a varying number of Cs (Fig. 3A) for the (8,3) functionalization chemistry. We find that disorder-induced D and IFM peak intensities change as a function of inter-G spacing, reaching an unexpectedly deep minimum when the spacing is 7 (Fig. 3, B and C). The SS and PL peak linewidth also show minimum values at that spacing (Fig. 3, D and E). These observations appear to be dependent on nanotube chirality as left- and right-handed (6,5)s functionalized by the same set of sequences yield different spectral patterns (fig. S7).

We offer a qualitative analysis of the data shown in Fig. 3. According to the mechanism of defect-induced Raman modes (*12*, *18*), the observed peak intensity is proportional to the extent of elastic electron scattering by defects. For the sequences used in our study we estimate that a SWCNT contains 1 to 5 guanine-modified sites per nanometer tube length based on molecular dynamics simulations of a typical DNA wrapping structure on a SWCNT (*15*). Because excitons are 2 to 3 nm in size (*19*) electron scattering is expected to involve multiple defect sites and is sensitive to not only the defect density but also the degree of order in the defect array. The minimum D and IFM peak intensities shown in Fig. 3 are thus interpreted as resulting from an ordered defect array generated by the 2G-7 sequence. This conclusion is also consistent with the observed minimum SS for the same sequence, as SS is another measure of disorder for semiconductors with isovalent substitution (*16*, *17*).

To independently evaluate the spectroscopy-derived result, we have applied single-particle cryo-EM to measure a 2G-7-(8,3) hybrid structure before and after functionalization. Cryo-EM imaging of 2G-7 functionalized (8,3) reveals filaments ~20 Å in diameter (fig. S11). In the nonfunctionalized structure coated with 2G-7, an averaged power spectrum from ≈ 2×10^5 images of particle segments yields no detectable features (fig. S12), implying a disordered DNA wrapping structure. In the functionalized structure we have detected a layer line pattern characteristic of a one-start helix with a 6.5 Å helical pitch visible from the averaged power spectrum of selected segments (Fig. 4A). The

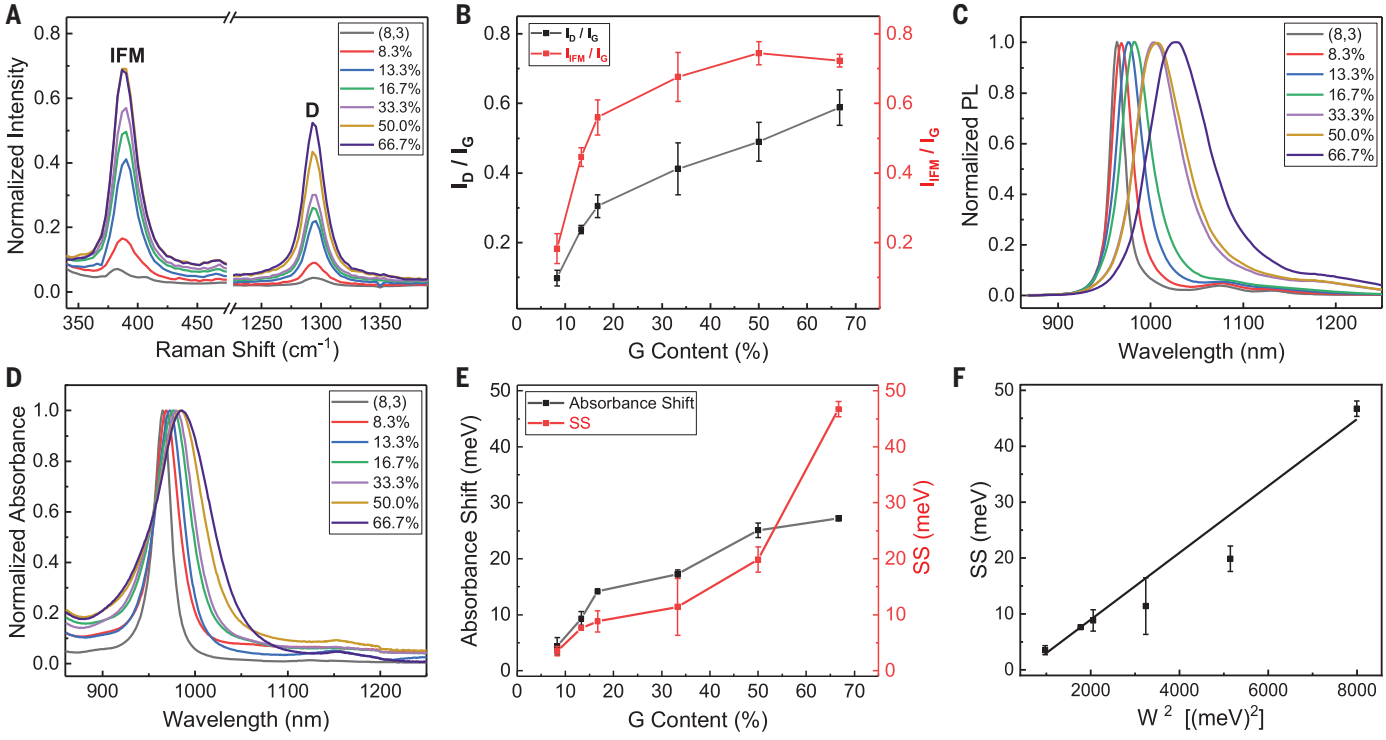

Fig. 2. Spectroscopic characterization of (8,3) functionalized with DNA of varying G content (see table S1 for sequence information). (**A** and **B**) IFM and D peak intensity (normalized by the intensity of the "G" peak) profile. (**C** and **D**) PL and absorbance profile. (**E**) Absorbance shift and SS profile. (**F**) SS versus W^2 and a linear fit (R^2 = 0.98) using Eq. 1 with T = 349.3 K. Error bars shown here and elsewhere in this work are derived from three independently measured values for each of three independently prepared samples. Spectra in (A) and (C), are measured with 671 nm excitation. See fig. S9 for original data.

helical structure is also visible in the 2D class average (Fig. 4B). Ab initio reconstruction—an unbiased and reference-free approach—was employed to generate a 3D reconstruction of the DNA-coated nanotube (Fig. 4C). Figure 4D shows a highly averaged version of that reconstruction, with an atomic model for the SWCNT. Because of the low signal-to-noise ratio in these cryo-EM images and the apparent lack of any other periodicities present, we have imposed a helical averaging of the density along the 6.5 Å pitch helix. The unfiltered 3D map (Fig. 4C) shows a coherence length of ~10 nm, shorter than the full length of the segments used. The density in Fig. 4, C and D, is shown as a left-handed helix although true handedness was not determined.

The 6.5 Å periodicity observed by cryo-EM provides support for the model of ordered defect array formation and is also a valuable clue regarding the mechanism of guanine functionalization. As discussed earlier, a correct reaction mechanism should yield a modified carbon that largely maintains its sp^2 character. Indeed, such chemistry has been well documented (*20*, *21*) and forms the basis for our proposal as shown in Fig. 4, E and F, and fig. S14B. Guanine oxidation by singlet oxygen has a plethora of pathways and products depending on reaction conditions and structural context but a common initial step is oxidation of the C_8 carbon on the imidazole ring (*22*). We propose that the C_8 carbon becomes electrophilic upon oxidation and then undergoes a 2+1 cycloaddition with a nearby C-C bond on a SWCNT to yield a three-membered ring. This is followed by C-C bond cleavage and concomitant ring opening as a result of ring strain, leaving C_8 to bridge the two carbons from the SWCNT and restore their sp^2 character. Theoretical calculations (*20*) predict that this type of reaction is most favorable on C-C bonds with large curvatures or bond strains, consistent with a previous observation from the guanine functionalization chemistry [figure 2C in (*6*)]. In (8,3) there are three types of C-C bonds with distinct curvatures; of these, C-C bonds along the helical armchair line shown in Fig. 4E possess the largest curvature. We note that the pitch (p) of this helical line has an intrinsic length scale of (8,3) determined solely by its chiral index (n, m) and C-C bond length a_c : $p = a_c\sqrt{n^2+m^2+nm}\ \frac{n-m}{n+m} = 6.45$ Å (for $a_c = 1.44$ Å), matching that observed by cryo-EM. We therefore propose a 2G-7 wrapping structure in which each of the 2Gs is covalently linked to a C-C bond along the armchair line, resulting in pinning of the DNA backbone along the same armchair line. Consistent with this functionalization-induced DNA pinning is our observation that 2G-5 and 2G-6 functionalized (8,3) also exhibit the same 6.5 Å helical pitch (fig. S13). Manual model building for 2G-7 functionalized (8,3) followed by energy minimization yields a model as shown in fig. S14A, in which two adjacent G modification sites are separated by five C-C bonds along the armchair line. This equal G spacing explains the minimum spectroscopy-derived structure disorder for 2G-7 functionalized (8,3).

In summary, we show that ordered SWCNT modification can be achieved by taking advantage of DNA sequence control over the spacing between adjacent reaction sites, and SWCNT's bond curvature–dependent reactivity. Our findings demonstrate the chemical feasibility of building a Little model. DNA-guided remodeling breaks the original symmetry of the nanotube lattice and therefore should lead to new modes of low-energy electronic excitation. Theoretical analysis shows that helical modification of a SWCNT in registry with its lattice may induce topological electronic behavior (*23*, *24*), suggesting that the chemistry we report here might be used to explore topological physics. We envision

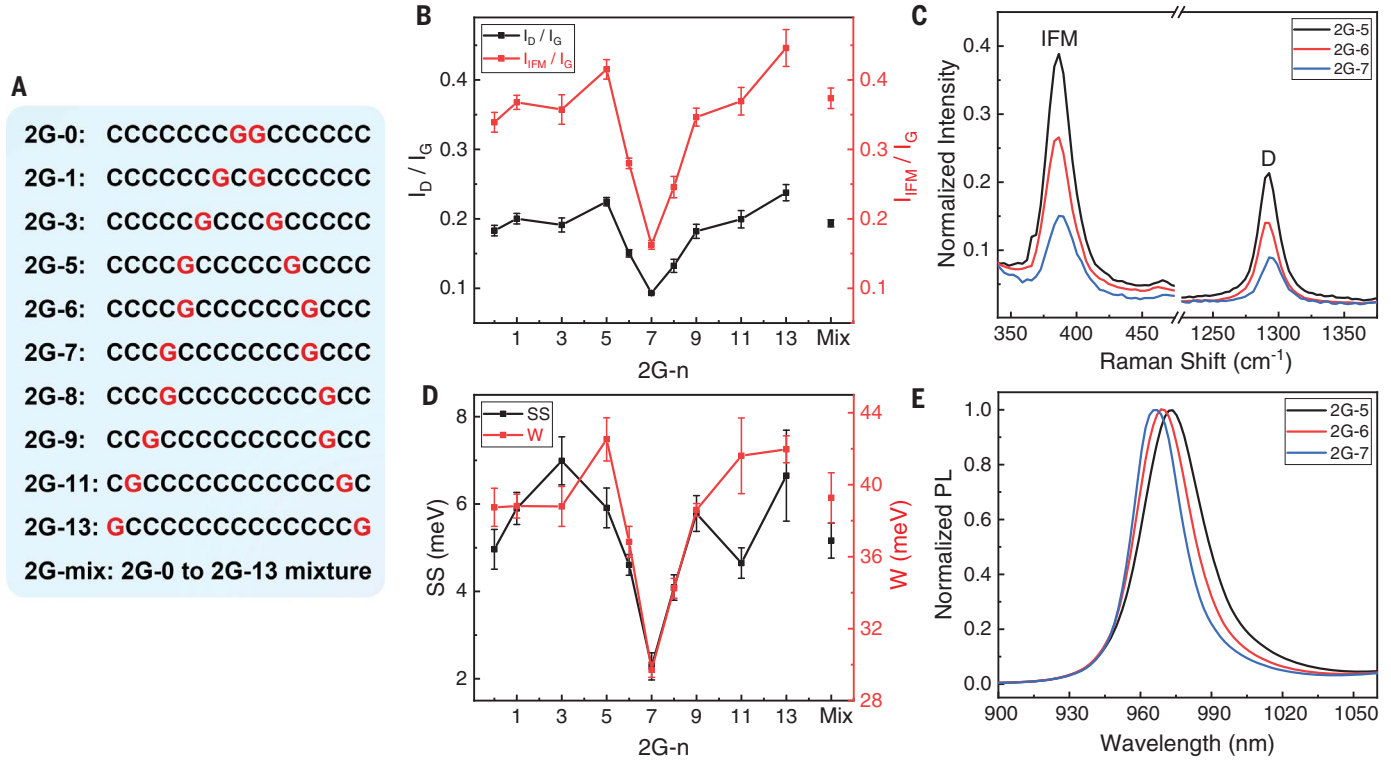

Fig. 3. Screening DNA sequences for the ordered defect array. (**A**) DNA sequence used for the screening. (**B**) D and IFM peak intensity profile. (**C**) Raman spectra of 2G-5, 2G-6, and 2G-7 functionalized (8,3) (normalized by the "G" peak). (**D**) SS and *W* profile. (**E**) PL spectra of the three samples. Spectra in (C) and (E) are measured with 671 nm excitation. See fig. S10 for original data.

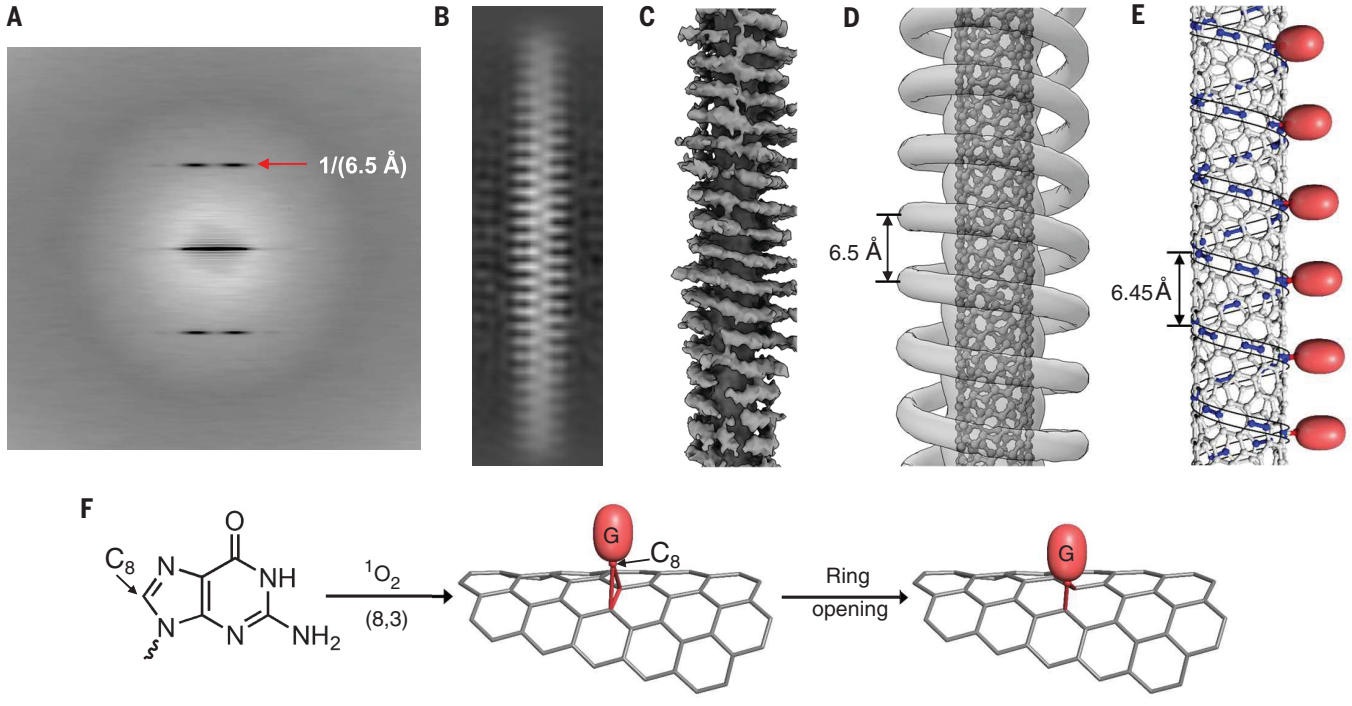

Fig. 4. Cryo-EM–derived structure model for 2G-7 functionalized (8,3) and reaction mechanism. (**A**) Averaged power spectrum from ~44,000 particles. Red arrow pointing to a layer line with a spacing of 1/(6.5 Å) from the equator. (**B**) Image of 2D class average. (**C**) Low-resolution 3D map generated by unbiased, reference-free approach displaying coherence that extends over an axial length of ≈ 10 nm. (**D**) 3D map corresponding to averaged density along the 6.5 Å pitch helix. (**E**) Carbon-carbon bonds that have maximum bond curvature, highlighted in blue along an armchair helical line of (8,3), along which every sixth carbon-carbon bond is modified by a guanine (red balls) according to modeling (fig. S14A). (**F**) A proposed reaction mechanism.

that future work will introduce diversity of functional groups, increase the coherent length of ordered modification, and eventually enable discovery of organic quantum materials and carbon-based, metal-free catalysts (*25*, *26*).

REFERENCES AND NOTES

1. W. A. Little, *Phys. Rev.* **134**, A1416–A1424 (1964).
2. D. Jérome, *Science* **252**, 1509–1514 (1991).
3. A. Hamo *et al*., *Nature* **535**, 395–400 (2016).
4. T. Kontos, *Nature* **535**, 362–363 (2016).
5. Y. Piao *et al*., *Nat. Chem.* **5**, 840–845 (2013).
6. Y. Zheng, S. M. Bachilo, R. B. Weisman, *ACS Nano* **13**, 8222–8228 (2019).
7. F. Yang *et al*., *Chem. Rev.* **120**, 2693–2758 (2020).
8. M. Zheng, *Top. Curr. Chem.* (*Cham*) **375**, 13 (2017).
9. Y. Zheng *et al*., *ACS Nano* **15**, 10406–10414 (2021).
10. J. K. Streit, J. A. Fagan, M. Zheng, *Anal. Chem.* **89**, 10496–10503 (2017).
11. N. Sato, Y. Tatsumi, R. Saito, *Phys. Rev. B* **95**, 155436 (2017).
12. A. Vierck, F. Gannott, M. Schweiger, J. Zaumseil, J. Maultzsch, *Carbon* **117**, 360–366 (2017).
13. T. Inaba, Y. Tanaka, S. Konabe, Y. Homma, *J. Phys. Chem. C* **122**, 9184–9190 (2018).
14. F. J. Berger *et al*., *ACS Nano* **13**, 9259–9269 (2019).
15. D. Roxbury, A. Jagota, J. Mittal, *J. Phys. Chem. B* **117**, 132–140 (2013).
16. M. Gurioli, A. Vinattieri, J. Martinez-Pastor, M. Colocci, *Phys. Rev. B Condens. Matter* **50**, 11817–11826 (1994).
17. M. Felici *et al*., *Phys. Rev. B Condens. Matter Mater. Phys.* **74**, 085203 (2006).
18. C. Thomsen, S. Reich, *Phys. Rev. Lett.* **85**, 5214–5217 (2000).
19. L. Lüer *et al*., *Nat. Phys.* **5**, 54–58 (2009).
20. Y.-S. Lee, N. Marzari, *Phys. Rev. Lett.* **97**, 116801 (2006).
21. A. Setaro *et al*., *Nat. Commun.* **8**, 14281 (2017).
22. Y. Ye *et al*., *J. Am. Chem. Soc.* **125**, 13926–13927 (2003).
23. V. I. Puller, S. V. Rotkin, *Europhys. Lett.* **77**, 27006 (2007) (EPL).
24. C. Hu, V. Michaud-Rioux, W. Yao, H. Guo, *Nano Lett.* **19**, 4146–4150 (2019).
25. K. Gong, F. Du, Z. Xia, M. Durstock, L. Dai, *Science* **323**, 760–764 (2009).
26. X. Liu, L. Dai, *Nat. Rev. Mater.* **1**, 16064 (2016).

ACKNOWLEDGMENTS

We thank B. Weisman and S. Tretiak for useful discussions. **Funding:** This work was supported by NIST internal funding and NIH GM122510 (to E.H.E.). Z.A.D. acknowledges an NRC postdoctoral fellowship. **Author contributions:** Z.L. and M.Z. conceived the idea. Z.L. and Z.A.D. performed the experiments, J.A.F. provided the samples, L.C.B. and E.H.E. performed cryo-EM and analysis, Z.L. and Y.L. performed the molecular modeling, T.A. and A.R.H.W. performed the Raman analysis, and Z.L., M.Z., L.C.B., and E.H.E. wrote the manuscript with input from all authors. **Competing interests:** The authors declare no competing interests. **Data and materials availability:** All data needed to evaluate the conclusions in the paper are present in the paper or the supplementary materials.

SUPPLEMENTARY MATERIALS

Submitted 5 February 2022; accepted 6 June 2022
10.1126/science.abo4628

DNA-guided lattice remodeling of carbon nanotubes

Zhiwei LinLeticia C. BeltránZeus A. De los SantosYinong LiTehseen AdelJeffrey A FaganAngela R. Hight WalkerEdward H. EgelmanMing Zheng

Science, 377 (6605),

Ordering surface modifications

Although several methods exist for functionalizing the surface of carbon nanotubes, the sites modified tend to be random. However, ordered functionalization of single-walled carbon nanotubes (SWCNTs) could lead to quantum properties. Lin *et al*. screened short DNA sequences containing cytosine (C) and guanine (G) to control the placement of G for photo–cross-linking reactions (see the Perspective by Wang). Spectroscopy and cryo–electron microscopy showed that for the (8,3)-SWCNT enantiomer, the sequences CGCGC regularly created an ordered helical structure with a 6.5-angstrom periodicity in which G bridges two carbon atoms. —PDS